CATRA: Interactive Measuring and Modeling of Cataracts

CATRA: Interactive Measuring and Modeling of Cataracts

Vitor F. Pamplona [1,2] Erick B. Passos[1,3] Jan Zizka[1,4] Manuel M. Oliveira[2]
Everett Lawson[1] Esteban Clua[3] Ramesh Raskar[1]

[1]MIT Media Lab [2]UFRGS Instituto de Informática [3]UFF Media Lab [4]Comenius University DAI

Abstract

We introduce an interactive method to assess cataracts in the human eye by crafting an optical solution that measures the perceptual impact of forward scattering on the foveal region. Current solutions rely on highly-trained clinicians to check the back scattering in the crystallin lens and test their predictions on visual acuity tests. Close-range parallax barriers create collimated beams of light to scan through sub-apertures, scattering light as it strikes a cataract. User feedback generates maps for opacity, attenuation, contrast and sub-aperture point-spread functions. The goal is to allow a general audience to operate a portable high-contrast light-field display to gain a meaningful understanding of their own visual conditions. User evaluations and validation with modified camera optics are performed. Compiled data is used to reconstruct the individual's cataract-affected view, offering a novel approach for capturing information for screening, diagnostic, and clinical analysis.

Keywords: cataracts; light-fields; computer-human interaction.

Links: DL PDF WEB VIDEO

1 Introduction

Cataracts are the leading cause of avoidable blindness worldwide. A cataract-affected eye scatters and refracts light before it reaches the retina. This is caused by a fogging or clouding of the crystallin. We measure this scattering by allowing one to compare a good light path with a path attenuated by the cataract. Our interactive and compact solution (called *CATRA*) goes beyond traditional cataract evaluation procedures by taking advantage of forward scattering to compute quantitative maps for opacity, attenuation, contrast, and point-spread function (PSF) of cataracts. The dissemination of devices with the ability to estimate intrinsic parameters of the eye may drive the development of future user-sensible technology for displays, rendering techniques, and improve our understanding of the human visual experience.

Cataracts are generally detected subjectively by locating a white reflex during a slit lamp examination. Research tools range from high-end Shack-Hartmann [Donnelly et al. 2004] and femtosecond optical coherence tomography systems [Palanker et al. 2010], to retro-illuminated image processing techniques [Camparini et al. 2000]. *CATRA* uses modified parallax barriers to create collimated beams of light to scan the crystallin lens (Figure 1). Placed close to the viewers' eye, the device ensures the beams are projected onto the fovea. Our patient-centric interactive approach, coupled with a simple optical setup, creates four comprehensive measurement maps. To verify their accuracy and precision, we cross-reference our results utilizing user studies and modified camera optics with partially masked diffusers. We go a step further reconstructing the individual experience of a cataract-affected view, previously unexplored by the graphics and vision communities.

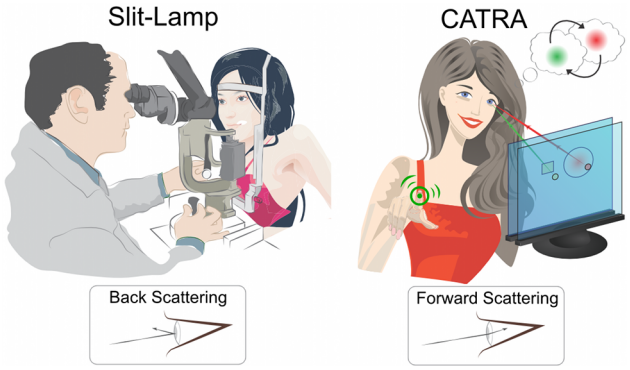

Figure 1: *Can we create a device that makes people aware of their early cataract condition? Using a light-field display, our method projects time-dependent patterns onto the fovea. Subject matches these alternating patterns that have passed through scattering (green) and clear (red) regions of the lens. An interactive software measures the attenuation and point-spread function across sub-apertures of the eye. Cataracts size, position, density, and scattering profile are then estimated.*

1.1 Contributions

We propose a novel optical design combined with interactive techniques to scan and measure the **forward scattering** of a cataract-affected lens without moving the users' visual point of reference by **creating steady images in the center of the fovea**. The main contributions of our paper include:

- A co-design of optics and user interaction that creates an effective solution to measure optical scattering inside the human eye. Mechanically moving parts are exchanged for moving patterns, on-screen, and forego the need to use external sensors. Off-the-shelf display and simple optical components make the device safe, cheap, and compact;
- Four interactive measurement techniques used to assess the size, position, attenuation, contrast, and point-spread function of scattering spots in imaging systems. These maps quantify and predict the scattering behavior inside the eye, and an image-based technique simulates the individual's eyesight.

The interactive technique efficiently reduces the search space for the PSF of a subject's eye. The captured data is more detailed than currently used techniques and no quantitative gold standard is established for in-vivo accuracy comparison. To our knowledge, this is the first method to interactively measure a sub-aperture PSF map of an eye, the first to measure sub-aperture contrast sensitivities, and the first to explore an individual cataract-affected view.

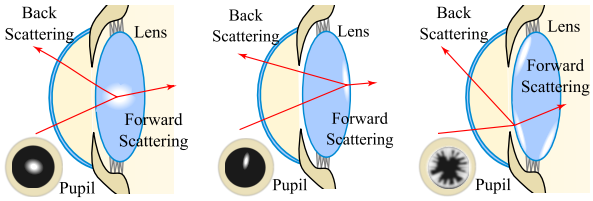

(a) Nuclear (b) Subcapsular (c) Cortical

Figure 2: *Most common types of cataracts: (a) Nuclear forms on the center of the crystallin, grows towards the periphery, and is strongly related to the aging process; (b) Sub-capsular starts on the back of the crystallin, mostly due to diabetes. (c) Cortical starts on the periphery, and grows inwards to its center. Back scattering reduces the visual acuity by partially blocking light. Forward scattering blurs the retinal image, decreasing contrast. Pupil size determines the strength of the effects.*

1.2 Related Work in Computer Graphics

Self-Evaluation Interactive Health-care Devices: This paper complements the contributions of NETRA [Pamplona et al. 2010], but aside from using interactive techniques to eye care, there are no other pertinent similarities. NETRA measures the *required optical correction and focal range* using static clip-ons for high-resolution displays. Our work computes the *spatial distribution of opacities* inside the crystallin lens and requires programmable high-contrast parallax barriers. NETRA's optics are designed to perform alignment tests, in which accommodation plays a critical role. *CATRA* relies on pattern matching and gaze control, where the alignment of the subject's eye is the main issue. Unlike NETRA, for which several devices provide similar measurements, there is no device capable of measuring quantitative maps for accuracy comparison.

Glare Studies and Light-Field Techniques: Isono et al. [1993] introduced dual-stacked LCDs to achieve programmable parallax barriers. We use a similar hardware setup to handle deficiencies in the human eye. A few researchers have addressed glare removal on coded aperture cameras by resampling the light field image [Raskar et al. 2008], separating the direct and global components [Talvala et al. 2007; Nayar et al. 2006], and adding an LCD to block the glare-affected part of the aperture [Hara et al. 2009]. Our research focuses on an indirect component measurement and glare estimation but applied to eyes. With our maps one can extend these works to correct images for cataract-affected eyes.

Simulation of a Subject's View: Several researchers have ray-traced schematic eyes in order to study the optical importance of each structure. Camp et al. [1990] developed a rendering technique that accounts for eye aberrations based on corneal topography. Kolb et al. [1995] introduced the realistic camera model for computer graphics producing a variety of optical effects. Mostafawy et al. [1997] designed a virtual eye for retinal image visualization using ray tracing techniques. Loos et al. [1998] ray-traced a schematic eye for best fit progressive lenses. Barsky [2004] used wavefront data to simulate the subject's vision. Deering [2005] models retinal cones and simulates the perception of displayed digital images. Pamplona et al. [2009] studied the pupil light reflex. Kakimoto et al. [2007] described wavefront tracing in the eye for refractive aberrations. Machado et al. [2010] created a model for the perception of color vision deficients. Schwiegerling et al. [2000] created a diffraction model for a standard eye, while [Ritschel et al. 2009] dynamically compute the PSF of a virtual eye, rendering glare effects in real-time. Although these works achieved their purpose, they did not test cataracts dysfunction; and most of them are not targeted toward the simulation of a specific individual's vision. Materials to simulate cataract effects were found, but they do not account for localized scattering [de Wit et al. 2006; Fine and Rubin 1999].

Techniques / Features	Opacity Map	Attenuation Map	Contrast Map	Sub-apert. PSFs	Scattering	Training Level
Slit Lamp	✓				Back	High
Scheimpflug	✓				Back	High
Retro Illum.	✓	✓			Fwd	Med
Shack-Hartmann	✓	✓		✓	Fwd	Low
OCTs	✓	✓			—	Med
Dynamic Light Scat.	✓	✓			—	High
CATRA	✓	✓	✓	✓	Fwd	Low

Table 1: *Comparison of our technique against current available technologies and research tools. We suspect that Shack-Hartmann, dynamic light scattering, OCTs and retro-illumination, coupled with image processing, are capable of generating maps comparable to ours, even though we are not aware of any such demonstration.*

2 Human Eye and Cataracts

Cataracts are denatured crystallin proteins that are clamped together in the nucleus, cortex or under the capsule of the crystallin (Figure 2). With the continuous production and accumulation of lens fibers throughout life, the crystallin becomes thicker and more compact. This disease is the leading cause of avoidable blindness worldwide [WHO 2005] and its occurrence is highly correlated to the aging process. 17% of the +40-year-old Americans have cataracts, 50% of +75-year-old have had cataracts, and its incidence is expected to grow with the increasing longevity [NIH-EDPRSG 2004; Li et al. 2010]. There is no efficient method to prevent it or to completely stop its growth. The rate of this expansion, however, can be controlled if early diagnostics are obtained [Fostera et al. 2003]. Methods to detect early cataracts and assess its progression over time could be potentially helpful for the development and testing of new treatments [Asbell et al. 2005], to alert patients, and to allow lifestyle adjustments to reduce further growth [Datiles et al. 2008].

Cataracts can be assessed by *backscattering* or *forward scattering* (Table 1). **Backscattering examination**: A slit-lamp microscope is used to backscatter light from cataract spots. It requires numerous focusing magnifications, angling and lighting possibilities and its reproducibility is very poor [Donnelly et al. 2004]; The Scheimpflug slit-lamp photography tilts the camera's depth of field to consistently get transversal sharp focused images of the lens. Cataracts appear as varied elevations in accordance to location and severity. Scheimpflug has the disadvantage of requiring many pictures, in different meridians, to reliably estimate the size of the opacity [Hayashi et al. 1998; Lasa et al. 1995].

Forward scattering examination: Retro-illumination techniques flood the retina with light, whose reflex reaches the crystallin from behind, propagating the scattering to the camera. Mean gray level, best fitting polynomials, feature extraction, and other image processing techniques are used to automatically measure size and shape of the cataract [Li et al. 2010]. Since the position of the spot is unknown, focusing skills are essential.

Research alternatives such as femtosecond lasers, and optical coherence tomography [Palanker et al. 2010] may provide new high-quality tools to estimate the size and position of a cataract. Using Shack-Hartmann, the coherent light ray hits the crystallin from behind and reaches the sensor. Blur captured by each lenslet is a sub-aperture PSF of the lens [Donnelly et al. 2004]. Shack-Hartmann uses infrared light, which may scatter differently than visible light. Cataracts can also be detected at the molecular level using dynamic light scattering [Ansari et al. 2000]. Although some of these techniques have been successfully used in clinics [Kim and Bressler 2009], their high costs limit the adoption for diagnostic purposes.

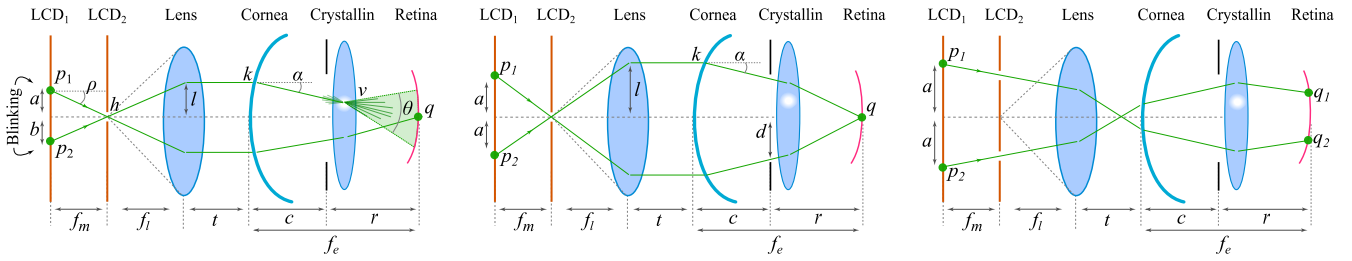

(a) Overall Concept (b) Pupil Size Measurement (c) Reference Points

Figure 3: *Cross-section of* CATRA *optical setup: (a) two stacked LCD and a lens create collimated beams of light. If a pinhole is drawn on LCD_2, all bright pixels on LCD_1 will focus at the same spot q on the retina. Thus LCD_1 defines the brightness of each retinal point, while LCD_2 controls the position and shape of q. (b) schematics for pupil size measurement. Subject chooses the biggest possible "a" while still seeing q; (c) schematics for showing reference points to control eye movement and gaze. The lens is positioned at one focal length (f_l) from the display. The distance f_m defines the angular resolution. All setups have a near-Lambertian lightbox placed behind LCD_1.*

3 Scanning the Crystallin Lens

We turn a parallax barrier into a time-dependent gaze-controlling scanning mechanism in order to explore the intrinsic parameters of the human eye. Figure 3 shows a diagram of the setup in flat-land and two applications. Two stacked LCDs create a programmable parallax barrier. An additional lens in front of the display increases light efficiency and reduces diffraction, creating collimated beams that converge to the same point on the retina. The device is positioned very close to the subject's cornea and its components are aligned with each other. The setup on Figure 3(a) traces light from each p_i through many regions of the crystallin, one p_i at a time. Each beam propagates the effect of possible occluders and imperfections to the central point of the fovea. The displayed image disappears on a mostly reflective cataract spot and scatters when the ray finds a semi-transmissive spot. Based on this setup, our method computes opacity, attenuation, contrast, and PSF maps of the eye using interactive perceptual pattern-matching functions, which compare clear-path light beams and scattered ones.

The intuition of our design relies on the role of each LCD: each pixel on LCD_1 maps to a region on the crystallin and each pixel on LCD_2 corresponds to a retinal position. Patterns drawn on LCD_2 are reflected on the retina, while the brightness of all pixels on LCD_1 are integrated on the same retinal point. A central pinhole in LCD_2 traces rays to the center of the fovea. Positions p_i (Figure 3(a)) inside the crystallin are a function of the angle ρ:

$$v(\rho) = f_l \tan\rho - c\tan\alpha, \tag{1}$$

where the bending angle α is defined by the optical corneal power in the point k. To create patterns on the subject's view, the pinhole on LCD_2 changes to the desired pattern. The position h on LCD_2 is mapped to the retina as (derived from compound lens equation):

$$q(h) = \frac{(-f_e^2 - f_e f_l)h}{f_l(-f_e - f_l + f_e t)} \tag{2}$$

Figure 4 illustrates our interactive 6-step method. After measuring the pupil size, which defines the discretization of the pupil area and enables the computation of the cataract size in meaningful physical units, we sequentially scan the subject's crystallin to identify the presence of cataracts. If this is found to be true, the subject marks the position of opacities and, in a posterior step, measures the light attenuation for each affected sub-aperture of the eye, thus creating opacity and attenuation maps. The measured attenuation values estimate the intensity of the sub-aperture PSF peak. The subject then performs perceptual pattern matching to measure the tail of the PSF. If the light attenuation is big, the tail may be bigger than the fovea, and its direct measurement is not reliable. Contrast-sensitivity tests approximate the PSF. This prefixed order of conducting the measurements is necessary to make the method viable.

Estimating Pupil Size: Figure 3(b) shows a simplified ray diagram to measure pupil size with two light beams in flatland. In practice, we display a circle with radius a of dots p_i on LCD_1 and a dot (pinhole) on the center of LCD_2. Parallel rays enter the eye and converge to a single point q on the fovea. Via interactive software, the subject increases a up to a point where the light rays are blocked by the iris and the projected pattern disappears (Figure 4(a)). The pupil radius is given by $d(a) = a - c\tan\alpha$, where c is the anterior chamber depth. We assume a circular pupil, thus the search is $1D$.

Screening for Cataracts: After subdividing the crystallin into testing regions, according to the pixel density of the LCD stack, Equation 1, and pupil size, we draw a single dot p_1 on LCD_1 and open a pinhole on LCD_2. Each move of p_1 scans a different region on the crystallin (Figure 4(b)). In this first scanning, p_1 is continuously changing position to cover the visible crystallin. Without pressing any keys the apparent sudden blinking or fading of the viewed pattern (e.g., case of p_2 in Figure 3(a)) reveals the presence of cataracts.

2D Scanning for the Opacity Map: If the subject sees a blinking or fading, the second scanning starts (Figure 4(c)). Software slows the frequency of changes in p_1 and allows the subject to mark faded regions by pressing keys. Since the subject does not see the pattern moving, audio feedbacks (beeps) indicate every change in p_1. When the scan covers the entire lens, an opacity map is built by concatenating the binary visibility functions for each sub-aperture. An hierarquical procedure for this scanning is left for future work.

Brightness Match for the Attenuation Map: The attenuation map measures the relative light attenuation across the crystallin. LCD_1 shows a pair of alternating dots (Figure 3(a)). p_1 is computed as the farthest point on the opacity map from the cataract spots. p_2 is a marked spot on the opacity map. Since both are projected on q at different time-slices, the subject sees similar patterns with oscillating brightness. At this point, the subject decreases the intensity level of the clear-path light beam and thus brighter p_1 until the oscillation stops (Figure 4(d)). This same task is executed for all marked regions on the opacity map. In the end, the attenuation map is built, showing the relative density of the cataracts.

Point-Spread Function Matching: Just like the brightness match, subject compares and matches alternating patterns p_i on LCD_1 (Figure 4(f)). Two patterns are drawn on LCD_2, one for each p_i. The former is a single pixel stimulus that hits the cataract spreading light onto the retina. The latter is a linear combination of a Gaussian and a box functions, which describes a sub-aperture PSF:

$$c(x) = \beta g(\sigma, x) + (1-\beta)p(x), \tag{3}$$

where β is a scaling factor defined by the measured attenuation value, σ is the standard deviation, g is a normalized Gaussian func-

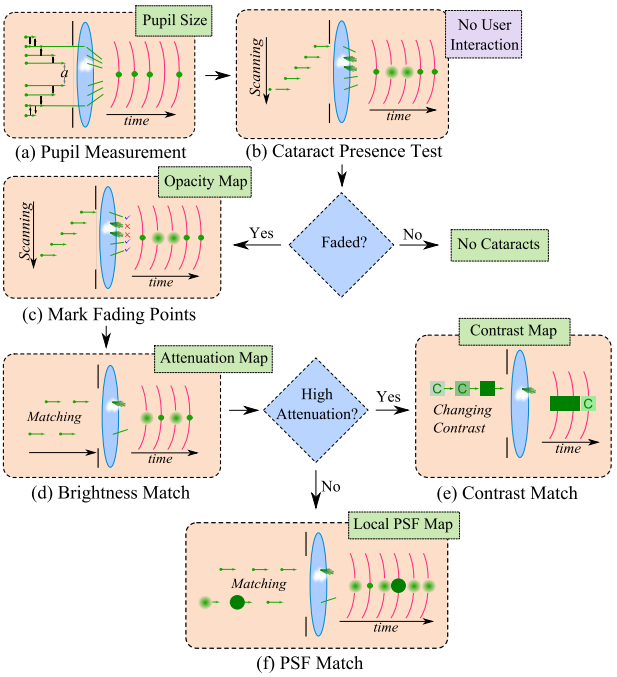

Figure 4: *Overall hierarchical method to efficiently measure cataracts. (a) Subject measures pupil size by increasing the distance a while perceiving the green dot. (b) Software automatically scans the lens to check for the presence of cataracts. (c) If a scattering spot is found, the scanning procedure is repeated with the subject's feedback. (d) By matching the brightness of two alternating paths of light we compute an attenuation map. (e) For a high scattering spot, the sub-aperture contrast-sensitivity test replaces the sub-aperture PSF measurement. In this case the subject increases the contrast of the displayed pattern up to a point where the letter becomes discernible. (f) sub-aperture PSF matching is the most detailed mapping, where the peak and Gaussian spread are measured for each scattering spot.*

tion and p is a normalized box function. In the absence of blur, $\beta = 0$. For each marked spot on the opacity map, the subject changes the values of σ to best match the visualized PSF .

Contrast-Sensitivity Test: A contrast sensitivity test is a replacement for the PSF measurement procedure. Wider PSFs project their tail out of the fovea and thus the subject may not be able to reliably measure it. For each attenuated sub-aperture, a single p_i is rendered on LCD_1 and a low-contrast 3 pixel-wide randomly-rotated letter **C** on LCD_2. In the beginning, user sees a white square. The subject increases the contrast until **C** becomes visible (Figure 4(e)). The rotation degree (0, 90, 180 or 270) of **C** is marked and noted. This visual acuity test is repeated for each marked sub-aperture, generating a complete map in the end.

3.1 Implementation Details

Gaze Control and Eye Position: Since all collimated beams are projected onto the fovea, no matter from which part of the cornea they enter the eye, the subject keeps looking to the same point and does not gaze. However, the subject can shift by the width of the pupil diameter, and remain seeing the same image. In order to overcome this, and keep the user in the same place, we draw reference points (Figure 3(c)) as a circular arrangement of patterns on LCD_2. Part of the circle disappears when the subject moves beyond a certain limit. With this technique, the subject can detect when she is off center, and should return to the original position.

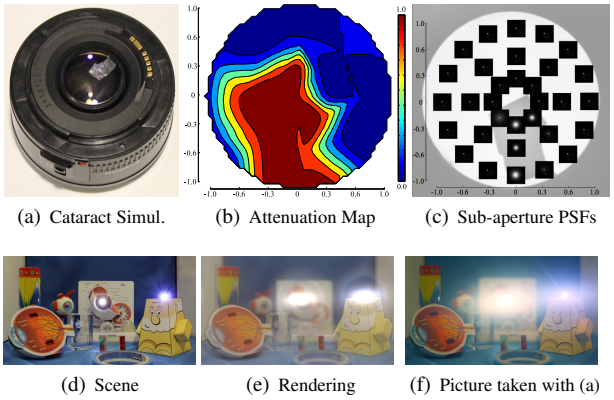

Figure 5: *We simulate strong cataracts by adding an 80-degree diffuser behind a $55mm$ lens of an SLR camera (a). We estimated an attenuation map (b) for an aperture of $2.2cm$ and a sub-aperture PSFs map (c) for an aperture of $3cm$. Using (d) as an input image and applying the measured PSFs from (c), we rendered the image (e) which shows similar effects to the picture taken with the cataract-simulated lens (f). Depth information is captured with a Z-camera (Microsoft Kinect).*

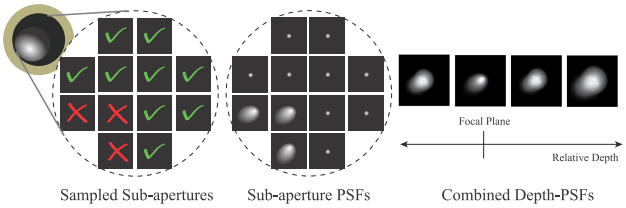

Figure 6: *Composition of lens' depth-dependent PSFs as the sum of all sub-aperture PSFs (center), shifted and combined in accordance with the relative depth from focal plane and the lens aperture (right). Check marks represent good light paths and Xs are scattering regions marked by the subject on the opacity map (left).*

System Resolution: Assuming h is a pinhole, the size of the cross section defined by the collimated light beams between the lens and the cornea is given by $s(p)f_l/f_m$, where $s(p)$ is the radius of the pattern p on LCD_1. Thus the bigger f_m, the smaller the beam radius is. The sampling resolution on the crystallin is defined by the discretization of the angle ρ (Equation 1), which is dependent on the pixel size on both LCD_1 and LCD_2. The retinal resolution is defined by pixel pitch on LCD_2 (Equation 2). To match the fovea (radius of $\approx 0.92mm$), light rays have to reach the cornea at maximum angle of $\rho = 2.12°$. Thus the biggest reliable pattern on LCD_2 has the radius of $f_l \tan(\rho)$.

Handling Accommodation and Refractive Errors: Our design does not allow multi-focus, such as NETRA [Pamplona et al. 2010]. We also do not assemble an image on the subject's retina as the standard parallax barrier does. The additional lens on top of the LCD plays an important role in handling accommodation. Subjects can focus on the image displayed by LCD_2 just like any other object seen through a lens. Refractive errors add variations to the position of the patterns on the retina, and can make the subject gaze, thus adding uncertainty to the cataract position inside the crystallin (e.g., if the scanning runs in circles and the subject has astigmatism, the method is actually measuring in an ellipsoidal shape).

4 Rendering the Subject's View

We propose an image-based approach for simulating the vision of a specific individual affected by cataracts. An accommodation-

Figure 7: *Rendering features using measured PSFs from a simulated cataract on a DLSR camera: (A) "Bokeh" effect, the cataract shape projected from out-of-focus bright light sources; (B) picture of the simulated cataract; (C) the estimated attenuation map; (D) the estimated PSF map; Cataract spots scatter light generating large glare patterns. Depth information captured from the z-buffer. Camera aperture of* $4mm$.

dependent convolution of sub-aperture PSFs simulates the view of a cataract-affected eye. We convolve depth-masked patches of the input image with their corresponding depth-dependent PSFs and combine the results into the final image. Each depth-dependent PSF is computed by combining the measured sub-aperture PSFs. Figure 6(right) illustrates how the combined PSF changes with accommodation. At the focal plane, all sub-aperture PSFs are just superposed and added, averaging their values. At depths away from the focal plane, the sub-aperture PSFs are shifted from the center according to the distance to the focal plane and the aperture, given by the pupil diameter. Computation of these depth-dependent PSFs can be defined by a sum over all sub-apertures:

$$PSF(B) = \sum_i PSF_i + B\overrightarrow{g_i} \tag{4}$$

where B is a depth-offset in diopters (reciprocal of the distance in meters $B = 1/d_m$) from the plane of focus defined by the accommodation, $\overrightarrow{g_i}$ is the vector that represents the shift of a given sub-aperture i from the center of the lens. The product $B\overrightarrow{g_i}$ models how the circle of confusion projected through i gets shifted from the center of the image as a function of depth. The final image is given by the sum of the depth-masked patches convolved with their respective PSFs for all depths in the scene:

$$IMG(A) = \sum h(A,B) \otimes PSF(B) \tag{5}$$

where $h(A,B)$ gives the depth-masked patch of the input image I for accommodation A in diopters and is defined pixel-wise by:

$$h_{x,y}(A,B) = \begin{cases} I_{x,y} & \text{if } depth(x,y) = A+B \\ 0 & \text{otherwise} \end{cases} \tag{6}$$

where $I_{x,y}$ is the intensity of the pixel x, y, and $depth$ is the distance from camera to the projected point x, y in diopters. Given sub-aperture PSFs, this depth-based approach renders artifacts which are similar to those described by cataracts-affected subjects, also computing the expected depth-of-field (Figure 5). To account for diffraction from the pupil, lens fibers and cataract opacities, we also added an augmented version of the glare model described in [Ritschel et al. 2009] to the computed PSF, including the attenuation map as an extra multiplication step to their aperture model. Figure 7 shows a simulated night-driving scene with the experimental data used to render it. Cataract shape (b) can be seen as a mask on the "bokeh" effect of the PSF composition.

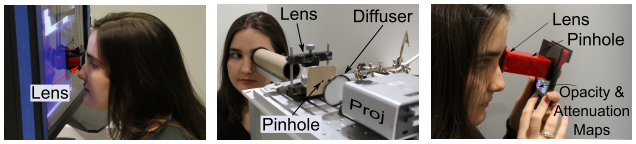

(a) Dual-LCD Monitor (b) DLP Proj.-Mask (c) Cell-Phone-Mask

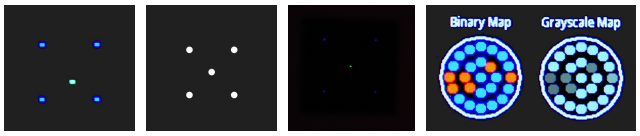

(d) LCD_1 (e) LCD_2 (f) View (g) Results

Figure 8: *Prototypes and a scanning procedure example: (a) stack of two LCDs from high-contrast low-resolution monochrome medical monitors; (b) a high-contrast DLP projector plus a pinhole mask, and (c) the cell phone LCD plus a pinhole mask. (d) a picture of the cell phone display on the scanning procedure. Blue dots are reference points. (e) the cell phone pinhole mask. The central pinhole performs the test while others allow for reference points. (f) a simulation for the subject's view (picture). (g) a picture of the cell phone screen showing the opacity and attenuation maps. Because of the absence of color filters, high contrast ratio and a better light box than standard LCDs, we consider (a) our best overall setup. (b) brightest and highest-contrast setup, which allows meaningful scattering projection through high density cataracts; and (c) it is the most portable, comprising of a clip-on for smart-phones.*

5 Prototypes and Evaluation

We explored different designs for Figure 3 that span across size, materials, interface, cost and static contrast. Figure 8(top) shows three of our prototypes. Our *Dual-LCD Monitor* is build using two 18" LCD TFT monochrome medical monitors stacked $f_m = 24mm$ apart, with brightness of $700cd/m^2$, contrast ratio of $550 : 1$, $90DPI$ ($280\mu m$ pixel pitch) and a 20-diopter lens, $50mm$ from the stack (Figure 8(a)). We use a single-pixel pattern on LCD_1 which reaches a scanning resolution of $510\mu m$ on the crystallin. Since these LCD panels do not have color filters, the aberrations are smaller than traditional monitors and the high static contrast gives a smaller residual light level for black pixels.

Since LCD_2 does not change for attenuation and opacity maps, by replacing it for a printed pinhole mask, we create a cheaper version of the same optics, which is still capable of measuring the opacity and attenuation maps, but cannot measure the contrast map or point-spread functions. This setup can be implemented as a clip-on for any high-contrast spatial light modulator. The *DLP Projector* prototype consists of a Mitsubishi PK10 pocket projector (DMD) and a 50×40mm diffuser as projection screen, at 800×600 in pixel resolution reaching $62\mu m$ in pixel pitch. A pinhole mask (pinhole radius of $100\mu m$) is placed $60mm$ away from the screen, and a 16-diopter lens is $62mm$ away from the mask. This setup uses a single-pixel pattern and has a scanning resolution of $56\mu m$ on the crystallin (Figure 8(b)). *Cell phone* setup uses a Samsung Behold II (180DPI or $141\mu m$ on pixel pitch - Figure 8(c)), with a static pinhole mask (pinhole radius of $100\mu m$) placed $40mm$ from the display, and a 25-diopter lens placed $40mm$ from the mask. Using a 3x3-pixels pattern on LCD_1, the scanning resolution is $370\mu m$ on the crystallin.

Masks are composed by 5 pinholes (Figure 8(e)), where the central one performs the measurement and peripheral ones allow for reference points. For instance, for a pupil radius of $\approx 1.5mm$, blue reference points drawn $5mm$ off-center reach the crystallin close to the pupil border and are projected at $0.3mm$ from the foveal center.

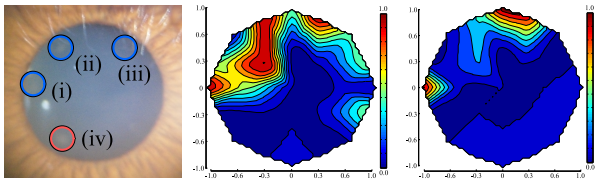

(a) Subject's Picture (b) Opacity Map (c) Attenuation Map

Figure 9: *Opacity and attenuation maps for one subject. (a) Picture of the cataract-affected eye. (b) Linear interpolated opacity map showing scattering regions highlighted by (i), (ii) and (iii). Spot (iv) cannot be found in our measurements. Attenuation map (c) resembles the opacity map and reveals a required increase of 70% on the red parts to allow the subject to observe the same intensity as a beam going through the center of eye. Subject was asked to rest between opacity and brightness matching tests, requiring a realignment of their position using the reference points.*

(a) Cataract (b) Opacity (c) Measured (d) Estimated (e) Difference

Figure 10: *Attenuation comparison for an entire round. Each pixel represents one estimation. (a) Shows the simulated cataract; (b) the estimated opacity map (c) pictures of each measurement spot; (d) estimated attenuation map and (e) difference between (c) and (d).*

5.1 Controlled Evaluation

Our methods are evaluated using a camera focused at infinity, with diffusers placed at the center of a compound DSLR lens, as shown in Figure 5(a). We manually change patterns seen through a live-view on a PC connected to the camera and find the parameter required for optimal matching. Each level of our method is validated independently of the others. For the accuracy tests, our maps are compared against pictures taken in each estimated position for attenuation and PSF maps. Canon 5D Mark II with $50mm$ lens, and C-mount Flea Camera from Point Grey Research with $16mm$ lens are used. Luminit diffusers with scattering angles of 5° ($7\times3mm$), 30° ($9\times4mm$) and 80° ($9\times4mm$) and a piece ($9\times6mm$) of a diffuse plastic bag are tested. Figure 5 shows the attenuation and PSF maps for a simulated cataract and its respective visual effects.

We test the accuracy of the estimated attenuation maps using the *DLP Proj. plus Mask* with the Flea Camera. Pictures of the scattered and free-path light beam were taken before the user adjusts the brightness levels. For 289 measurement spots in 7 rounds randomizing diffusers, the accuracy of the attenuation levels in absolute average error is $1.03\% \pm 4.20\%$. Figure 10 shows opacity and attenuation maps for one round. Contrast-sensitivity maps were estimated using the *Dual-LCD Monitor* with the Canon 5D. The repeatability of the contrast value (Range $[0,1]$) has an average error of 0.03 ± 0.03 for 116 measurements on 4 rounds.

PSFs maps were computed for the 80° and 5° diffusers. Using the Dual-LCD Monitor with a Canon 5D, the repeatability of the measurements in 128 tests points (4 rounds) is 0.03 ± 0.13 in normalized scale. PSF maps also represent position and size of a cataract. The 80° of $36mm^2$ was measured having $34mm^2 \pm 4.27$ and the 5° of $21mm^2$ having $29mm^2 \pm 8.55$ (Figure 11(a)). Repeatability for the diffuser's centroid is $0.01mm \pm 0.01$, computed by:

$$C = \frac{\sum a_i \overrightarrow{g_i} o_i}{\sum o_i} \tag{7}$$

where a_i and o_i are the i-th attenuation and binary opacity values.

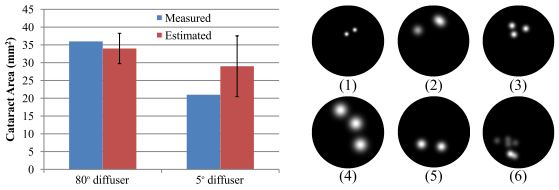

(a) Camera Cataracts (b) Volunteer Results

Figure 11: *Accuracy comparison for size with two simulated cataracts on cameras (a) and a repeatability analysis in position (b) for subjects of Table 2. Each Gaussian represents the centroid (Equation 7) of the measured maps for one round with its σ as the standard deviation of centroids throughout subject's maps. The black disk represents the pupil size. (b) shows good repeatability for (1, 3, 6), reasonable for (2,5) and very poor on (4).*

S	Size	Centroid	Compensation
1	1.16 ± 0.07	$(\ 0.14, -0.45) \pm 0.23$	
2	0.68 ± 0.09	$(-0.06, -0.85) \pm 0.53$	$146\% \pm 12.29$
3	0.64 ± 0.15	$(-0.06, -0.57) \pm 0.35$	
4	0.36 ± 0.21	$(\ 0.21, -0.31) \pm 0.74$	$136\% \pm 2.77$
5	0.27 ± 0	$(-0.08,\ \ 0.45) \pm 0.52$	
6	0.45 ± 0.12	$(-0.43,\ \ 0.82) \pm 0.38$	$135\% \pm 6.9$

Table 2: *Estimated size (mm^2), position off-center (mm) and attenuation values for 5 early cataract-affected volunteers ($1\text{-}5^{th}$) plus the scratched contact lenses (6^{th}). The compensation values show how much brighter the light ray that passes through the scattering region must be to match the intensity of a clear light path.*

PSF tests took $\approx 7min$ for full 36-sub-aperture maps on cameras.

Cataract-induced contact lenses: We scratched a contact lens in a zig-zag-line pattern, generating a $\approx 0.5mm^2$ ($0.5\times1mm$) scattering region. Subject measured opacity and attenuation maps 9 times. The estimated size is $0.45mm^2 \pm 0.12$ at $(-0.43, 0.82)mm \pm 0.38mm$ off-center. Average result for attenuation maps indicates the need of $135\% \pm 6.9$ of the brightness for the points going through the scratch when compared with clear-path brightness. Measurements were taken under a pupil radius of $\approx 1.8mm$. We notice that, the contact lens may rotate when subject blinks during the test. Tests were made using reference points (Figure 3(c)).

5.2 User Evaluation

18 subjects tested our cell-phone-based prototype. Each subject took the test twice for training, and at least twice for data collection. 5 early cataract-affected volunteers (ages 68 to 76 plus one 30-year-old) trained for $\approx 10min$ and tested for $\approx 10-15min$. Subjects with no cataract took $3min$ on training and testing sessions. A single screening round for the opacity map (no user interaction) runs in $10secs$. Each map measures the observed attenuation for 24 testing points. Estimated values are shown in Table 2 and Figure 11(b). Figure 9 shows the estimated opacity and attenuation maps for a volunteer compared with a picture of his eye. Additionally, 14 healthy eyes were scanned and no cataract was found. Quantitative accuracy tests comparing our maps against slit-lamp pictures could not be reliably performed because of low-quality slit-lamp pictures. All tests were made using reference points to control eye motion. Our user study was performed according to approved procedures for human subjects, and employing de-identified volunteers.

For these experiments, we assume no optical aberrations (the person takes the test wearing his corrective lenses, if (s)he uses some) and a thin lens system (lens with negligible thickness). Thus, α in Equation 1 can be approximated by $\tan\alpha = l/f_e$, where f_e is the axial length of the eye, which is the reciprocal of the optical power at point k. $f_e = 25mm$ and $c = 3.15mm$ in our calculations.

6 Discussion and Conclusion

We presented an interactive method coupled with an optical design to detect early cataracts in the human eye using view-dependent high-contrast displays. Early cataracts are a relevant global health problem that previously required highly-trained technicians and cumbersome equipment to be detected. This innovation measures the forward scattering profile and creates the PSF of the crystallin with no need of a coherent light source and no mechanical apparatus. *CATRA* ensures the projection of pattern directly onto the fovea to avoid gazing issues. Users look through an eyepiece and interact with a keypad based on what they see. Our interactive method scans the subject's crystallin lens to estimate opacities, attenuation levels, contrast-sensitivity, and sub-aperture point-spread functions. Section 5.1 validates the optics of the device and the implemented mathematical models. Small variations in attenuation (1%), contrast (3%) and PSF (3%) maps indicate the consistency of our technique. User-driven validation experiments attested the precision of the method (maximum $\sigma = 0.2mm^2$ in size, $\approx 2\%$ of the pupil area), the forward scattering feature (estimated attenuations on $\approx 140\%$), the gaze control mechanism of the optical design (maximum $\sigma = 0.7mm$ in position, $\approx 20\%$ of the pupil diameter), and the stability of the foveal projection on early cataract-affected elderly subjects (Section 5.2). We believe the quantitative results of our new patient-centric interaction-based method are first of its kind, with no currently available device producing comparable data. Reasonable repeatability rate and the complete absence of false positives, required for screening tools, are incentives to continue this investigative research.

We go a step further creating tools to understand a cataract-affected visual experience, that remained unexplored by the graphics and vision communities. Simple presence of opacities might already indicate glare issues, but a complete contrast, or PSF map, can give a more detailed profile of the effects on scenes with high dynamic ranges. A PSF mapping tool provides a new opportunity for doctors and patients. Renderings help to mitigate this relationship through a shared visual experience, opening a dialogue to further assess and aid the diagnosis of developing cataracts.

Limitations: Since *CATRA* requires active user participation, we are limited by the subject's ability to follow instructions. By using perceptual judgement and pattern matching, the technique does not work if a uniform-scattering cataract covers all the visible crystallin, as in advanced cases of the disease. Such uniformity could offset the attenuation and PSF maps. For the opacity map, subjects would see dim patterns at all times, being challenging to mark scattering regions. The contrast map, however, should remain accurate, since the measured low contrast would be all over the lens.

Pupil size may vary during the test, but these variations are estimated to be very small since the patient's eye is covered by an eyecup. Retinal diseases may augment the results. Just like standard-wavefront-aberration maps of the eye, our maps do not reveal aberration's depth. It's acceptable, however, that a screening tool find conditions other than the target one. Although the method is sensitive to refractive aberrations, this can be solved by taking these aberrations into account and pre-warping light rays. Further clinical studies with wavefront aberration maps are required to precisely estimate their impact. According to our experience, a few degrees of myopia moves the projection in circles.

The dual-stacked-LCD shares some limitations of other similar designs such as decrease in brightness, and predefined viewing zones [Dodgson 2009]. The time-dependent nature of the solution removes crosstalk. The map resolution is a function of pixel density, distance between LCDs screens, and the distance from the display to the eye. Current effective static contrast on LCDs may influence the ability to discern the projected patterns and measure the PSF. These limitations still allow the user to obtain reliable, repeatable results using our technology.

Experiences shared on the user tests: Many volunteers were fascinated by their opacity map on the screen of a smart-phone. One of the cataract-affected subjects has reported difficulty in explaining the visual effects to his family. A simple rendering tool may address these communication issues between them. Response from the local community has been very positive. Our data shows a reasonable repeatability, but some users found the alignment task using reference points difficult to understand. According to Don Yansen, CEO of Click Diagnostics that provides affordable health care in developing countries, "Village health workers will be able to cheaply and quickly flag early stage cataracts and macular degeneration in order to refer individuals to hospitals, where their vision can be restored before they effectively become blind". During our research, one of the authors was able to self-diagnose his cataract that went undetected during his eye-exam a few months before the submission and was confirmed afterwards.

Reactions from ophthalmologists: Several researchers and local practicing ophthalmologists have been in collaboration with this project, and are enthusiastic about its quantitative outcomes. Many of them have experimented with the device, and the general response has reinforced that reliable quantitative measurements for cataracts are already very helpful for screening purposes. One of them commented on their experience that the Shack-Hartmann wavefront sensor to measure high-order optical distortions of the human eye had no practical application twenty years ago. Today, the high accuracy of these devices provide the only reliable data for the LASIK surgery. Widespread availability of devices like ours, which generate quantitative data about cataracts, may benefit the future of diagnostic and surgical practice. Since cataracts are correlated with macular degeneration [Liu et al. 1989], many doctors have suggested the use of this device as a side screening tool for other visual impairments. A few ophthalmologists we have been discussing with, reported strong concerns about the complete absence of a glare disability test in order to obtain a driver's license. For instance, visual acuity tests, in general, do not assess for glare and night driving effects, while simple and cheap tests such as ours, would reveal currently unchecked impairments. Our overall goal is to create tools that empower self-awareness about commonly unscreened health condition of the eye. We stress that this device does not directly diagnose or treat for cataracts, but in the future, methods like this might be able to give a complete summary of visual performance. Our hope is that these results encourage more people to design and develop interactive tools which will augment the understanding of the human visual experience.

Acknowledgments

We would like to thank doctors Bruce Moore, Rob Pocaro, Yvvone Tsai, Shrikant Bharadwaj, Fabiano Cade, and Caio Regatieri for sharing their thoughts on the clinical use for this device. Frédo Durand, Bill Freeman, Sam Hasinoff, Ankit Mohan, Leandro Fernandes, Mahdi Mohammad-Bagher, and Kartic Subr for their comments on an earlier draft of the paper. All the SIGGRAPH reviewers for their thorough and insightful feedback. Tiago Oliveira for the illustration on Figure 1, Tyler Hutchison for the voice-over and the entire Camera Culture group for their unrelenting support; Vitor and Manuel acknowledge CNPq-Brazil fellowships 142563/2008-0, 200763/2009-1, 200284/2009-6, 308936/2010-8, 480485/2010-0. Jan is supported by Comenius University and ME-Inspection. Erick acknowledges CAPES-Brazil scholarship BEX 2529-10-6. Ramesh is supported by an Alfred P. Sloan Research Fellowship, and Esteban by a Young Scientist of Rio de Janeiro Fellowship.

References

ANSARI, R. R., DATILES, M. B., AND KING, J. F. 2000. A new clinical instrument for the early detection of cataract using dynamic light scattering and corneal topography. *SPIE Ophthalmic technologies X 3908*, 38–49.

ASBELL, P. A., DUALAN, I., MINDEL, J., BROCKS, D., AHMAD, M., AND EPSTEIN, S. 2005. Age-related cataract. *The Lancet 365 (9459)*, 599–609.

BARSKY, B. A. 2004. Vision-realistic rendering: simulation of the scanned foveal image from wavefront data of human subjects. In *APGV 2004*, 73–81.

CAMP, J., MAGUIRE, L., AND ROBB, R. 1990. An efficient ray tracing algorithm for modeling visual performance from corneal topography. In *Vis. Biomed. Comp.*, 278 –285.

CAMPARINI, M., MACALUSO, C., REGGIANI, L., AND MARAINI, G. 2000. Retroillumination vesus reflected-light images in the photographic assessment of posterior capsule opacification. *Invest. Ophthalmol. Vis. Sci 41*, 10, 3074–3079.

DATILES, M. B., ANSARI, R. R., SUH, K. I., VITALE, S., REED, G. F., JR, J. S. Z., AND FERRIS, F. L. 2008. Clinical detection of precataractous lens protein changes using dynamic light scatterin. *Arch. Ophthalmol. 126(12)*, 1687–1693.

DE WIT, G. C., FRANSSEN, L., COPPENS, J. E., AND VAN DEN BERG, T. J. 2006. Simulating the straylight effect of cataracts. *J. Cataract Refract Surg. 32*, 294–300.

DEERING, M. F. 2005. A photon accurate model of the human eye. In *SIGGRAPH*, vol. 24(3), 649–658.

DODGSON, N. 2009. Analysis of the viewing zone of multi-view autostereoscopic displays. In *SPIE Stereoscopic Displays and Applications XIII*, vol. 4660, 254265.

DONNELLY, W. J., PESUDOVS, K., MARSACK, J. D., SARVER, E. J., AND APPLEGATE, R. A. 2004. Quantifying scatter in shack-hartmann images to evaluate nuclear cataract. *Journal of refractive surgery 20(5)*, S515–S522.

FINE, E. M., AND RUBIN, G. S. 1999. Effects of cataract and scotoma on visual acuity: A simulation study. *Optometry and Vision Science 76(7)*, 468–473.

FOSTERA, P. J., WONG, T. Y., MACHIN, D., JOHNSON, G. J., AND SEAH, S. K. L. 2003. Risk factors for nuclear, cortical and posterior subcapsular cataracts in the chinese population of singapore. *Br J Ophthalmol 87*, 1112–1120.

HARA, T., SAITO, H., AND KANADE, T. 2009. Removal of glare caused by water droplets. In *CVMP*, 144–151.

HAYASHI, K., HAYASHI, H., NAKAO, F., AND HAYASHI, F. 1998. In vivo quantitative measurement of posterior capsule opacification after extracapsular cataract surgery. *Am J Ophthalmol 125*, 837–843.

ISONO, H., YASUDA, M., AND SASAZAWA, H. 1993. Autostereo-scopic 3-D display using LCD-generated parallax barrier. *Electr. and Comm. in Japan 76(7)*, 7784.

KAKIMOTO, M., TATSUKAWA, T., MUKAI, Y., AND NISHITA, T. 2007. Interactive simulation of the human eye depth of field and its correction by spectacle lenses. *Comp. Graph. Forum 26*, 627–636.

KIM, S., AND BRESSLER, N. M. 2009. Optical coherence tomography and cataract surgery. *Curr Opin Ophthalmol 20*, 46–51.

KOLB, C., MITCHELL, D., AND HANRAHAN, P. 1995. A realistic camera model for computer graphics. In *ACM SIGGRAPH*, 317–324.

LASA, M., DATILES, M., MAGNO, V., AND MAHURKAR, A. 1995. Scheimpflug photography and postcataract surgery posterior capsule opacification. *Ophthalmic Surg. 26*, 110–113.

LI, H., LIM, J. H., LIU, J., MITCHELL, P., TAN, A. G., WANG, J. J., AND WONG, T. Y. 2010. A computer-aided diagnosis system of nuclear cataract. *IEEE Trans. Bio. Eng. 57(7)*, 1690–1698.

LIU, I., WHITE, L., AND LACROIX, A. 1989. The association of age-related macular degeneration and lens opacities in the aged. *Am.J. of Public Health 79(6)*, 765–769.

LOOS, J., SLUSALLEK, P., AND SEIDEL, H.-P. 1998. Using wavefront tracing for the visualization and optimization of progressive lenses. *Comp. Graph. Forum 17*, 255–265.

MACHADO, G. M., AND OLIVEIRA, M. M. 2010. Real-time temporal-coherent color contrast enhancement for dichromats. *Comp. Graph. Forum 29*, 3, 933–942.

MOSTAFAWY, S., KERMANI, O., AND LUBATSCHOWSKI, H. 1997. Virtual eye: Retinal image visualization of the human eye. *IEEE CGA 17*, 8–12.

NAYAR, S., KRISHNAN, G., GROSSBERG, M. D., AND RASKAR, R. 2006. Fast separation of direct and global components of a scene using high frequency illumination. *ACM TOG 25(3)*, 935–944.

NIH-EDPRSG. 2004. Prevalence of cataract and pseudophakia/aphakia among adults in the united states. *Arch Ophthalmol 122*, 487–494.

PALANKER, D. V., BLUMENKRANZ, M. S., ANDERSEN, D., WILTBERGER, M., MARCELLINO, G., GOODING, P., ANGELEY, D., SCHUELE, G., WOODLEY, B., SIMONEAU, M., FRIEDMAN, N. J., SEIBEL, B., BATLLE, J., FELIZ, R., TALAMO, J., AND CULBERTSON, W. 2010. Femtosecond laser-assisted cataract surgery with integrated optical coherence tomography. *Science Translational Medicine 2*, 58, 58ra85.

PAMPLONA, V. F., OLIVEIRA, M. M., AND BARANOSKI, G. 2009. Photorealistic models for pupil light reflex and iridal pattern deformation. *ACM TOG 28(4)*, 106.

PAMPLONA, V. F., MOHAN, A., OLIVEIRA, M. M., AND RASKAR, R. 2010. Netra: interactive display for estimating refractive errors and focal range. *ACM TOG 29(4)*, 77:1–77:8.

RASKAR, R., AGRAWAL, A., WILSON, C. A., AND VEERARAGHAVAN, A. 2008. Glare aware photography: 4d ray sampling for reducing glare effects of camera lenses. In *ACM SIGGRAPH*, 56:1–56:10.

RITSCHEL, T., IHRKE, M., FRISVAD, J. R., COPPENS, J., MYSZKOWSKI, K., AND SEIDEL, H.-P. 2009. Temporal glare: Real-time dynamic simulation of the scattering in the human eye. *Comp. Graph. Forum 28*, 2, 183–192.

SCHWIEGERLING, J. 2000. Theoretical limits to visual performance. *Survey of ophthalmology 45*, 2, 139–146.

TALVALA, E.-V., ADAMS, A., HOROWITZ, M., AND LEVOY, M. 2007. Veiling glare in high dynamic range imaging. *ACM TOG 26(3)*.

WHO, 2005. State of the world's sight: Vision 2020, the right to sight: 1999-2005.